Refracted arrival waves in a zone of silence from a finite thickness mixing layer

Takao Suzuki[a)] and Sanjiva K. Lele

Department of Aeronautics and Astronautics, Stanford University, Stanford, California 94305-4035

Refracted arrival waves which propagate in the zone of silence of a finite thickness mixing layer are analyzed using geometrical acoustics in two dimensions. Here, two simplifying assumptions are made: (i) the mean flow field is transversely sheared, and (ii) the mean velocity and temperature profiles approach the free-stream conditions exponentially. Under these assumptions, ray trajectories are analytically solved, and a formula for acoustic pressure amplitude in the far field is derived in the high-frequency limit. This formula is compared with the existing theory based on a vortex sheet corresponding to the low-frequency limit. The analysis covers the dependence on the Mach number as well as on the temperature ratio. The results show that both limits have some qualitative similarities, but the amplitude in the zone of silence at high frequencies is proportional to $\omega^{-1/2}$, while that at low frequencies is proportional to $\omega^{-3/2}$, ω being the angular frequency of the source. © *2002 Acoustical Society of America.* [DOI: 10.1121/1.1428265]

PACS numbers: 43.28.Py, 43.28.Ra [MSH]

I. INTRODUCTION

Suppose an acoustic source is located in a slower medium, but adjacent to a faster medium. The slower or faster medium refers to the medium whose propagation speed is slower or faster than for the other (see Fig. 1). In such a case, there may exist a path arriving at the observer located in the slower medium which takes shorter time than direct waves; namely, once the ray arrives at the surface of the faster medium, propagates along it, and departs from it toward the observer. As the Fermat's principle indicates, under such a condition, actual waves propagate along this ray path, referred to as "refracted arrival waves,[1–3]" or sometimes as "head waves,[4]" or "lateral waves,[5]" etc.

The formula of refracted arrival waves can be derived using a contour integral when the interface between the two media can be treated as discontinuous. This case is considered to be a low-frequency limit in a sense that the acoustic wavelength is much longer than the thickness of the interface. However, when the acoustic wavelength becomes much shorter than the thickness of the interface, the low-frequency formula tends to underpredict the amplitude of refracted arrival waves. Instead, one should rather analyze these waves based on geometrical acoustics, namely, the high-frequency limit. Such distinction could be important in jet-noise problems (see Fig. 2) as described in this paper.

When a noise source is located right below or even inside a mixing layer, there exists a region in which direct waves from the source cannot reach, referred to as the "zone of silence." Instead of direct waves, secondary waves occupy this region. In two dimensions, these waves are particularly expressed in the form of general plane waves. These waves are generated by disturbances of direct waves on the other side of the mixing layer. The formula of such waves was derived by Gottlieb[1] using a contour integral assuming a vortex sheet; however, the thickness of the mixing layer, in many realistic cases, can be equivalent to or longer than the acoustic wavelength of the sound radiated from jets.[6] In other words, the high-frequency sound in the zone of silence should not be estimated using a discontinuous interface model.

The purpose of this paper is to clarify the difference between the low- and high-frequency limits of refracted arrival waves from a transversely sheared mixing layer. By assuming that the thickness of the mixing layer is finite and the velocity and temperature profiles approach the uniform free-stream conditions exponentially, ray trajectories are asymptotically solved. Furthermore, a formula for pressure amplitude can be explicitly derived as a far-field asymptote using the Blokhintzev invariant[7] in the high-frequency limit. Unlike direct waves, refracted arrival waves cannot be derived using a stationary-phase-type method.[8] Note that at high frequencies, instability waves inherent in a mixing layer do not directly influence the noise radiation. In fact, dominant high-frequency noise sources exist relatively close to the jet exit in which the vortical disturbance level is relatively low.[9] Hence, the solution of refracted arrival waves from a finite thickness mixing layer should contain the basic mechanism of the high-frequency sound in the zone of silence for jet-noise problems. This study also indicates that the amplitude is fairly sensitive to the spreading rate of the mixing layer in reality.

The comparison between the low- and high-frequency limits demonstrates that as the frequency increases, the amplitude of refracted arrival waves tends to become larger than the prediction based on a vortex sheet. The key difference is that as the frequency varies, the low-frequency formula behaves as $\sim (\omega x)^{-3/2}$, while the high-frequency formula behaves as $\sim \omega^{-1/2} \alpha^{-1} x^{-3/2}$. (Here, ω denotes the angular frequency of the source, α denotes the exponential factor of either the velocity or temperature profile, which only de-

---
[a)]Current address: Division of Engineering and Applied Science, California Institute of Technology, Pasadena, California 91125
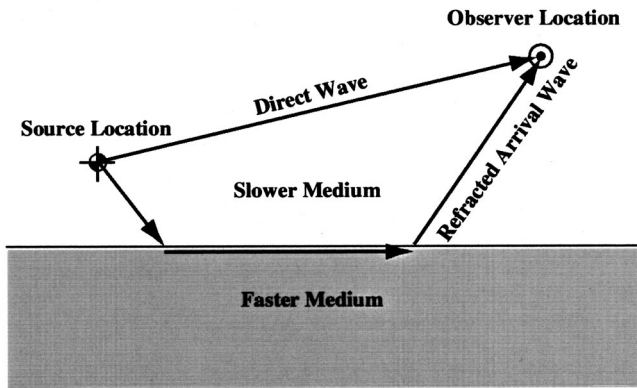
FIG. 1. Schematic of the paths of a refracted wave and a direct wave.

FIG. 3. Schematic of the coordinate system of a two-dimensional mixing layer.

pends on the flow geometry, and x denotes the distance from the source in the flow direction.) In addition, the dependence on the Mach number and the temperature ratio as well as the source location is numerically investigated based on geometrical acoustics, and it is compared with the analytical expressions. It is observed that the analytical expression approximates the amplitude fairly well even if the source is located inside the mixing layer. Through this study, the sound radiation in the zone of silence at high frequencies can be understood in the context of jet-noise problems.

The outline of this paper is as follows: After the Introduction, the formulas of refracted arrival waves in the high-frequency limit are derived, and those in the low-frequency limit are also revisited. In Sec. III, numerical procedures of geometrical acoustics are described. Next, the analytical formulas and the numerical results are compared in Sec. IV; the conclusions are presented in Sec. V.

II. DERIVATION

Consider a two-dimensional, transversely sheared mixing layer. Take x to be the flow direction and y to be the vertical direction, and set M_- and a_- to be the free-stream Mach number and the speed of sound on the lower side, and M_+ and a_+ to be those on the upper side, respectively (see Fig. 3 for a schematic). In this paper, the subscript $-$ denotes the lower side, and $+$ the upper side. Assume that the Mach number and temperature profiles do not change in the x direction, and the mean pressure is constant everywhere (note that the effects of mixing layer spreading are discussed at the
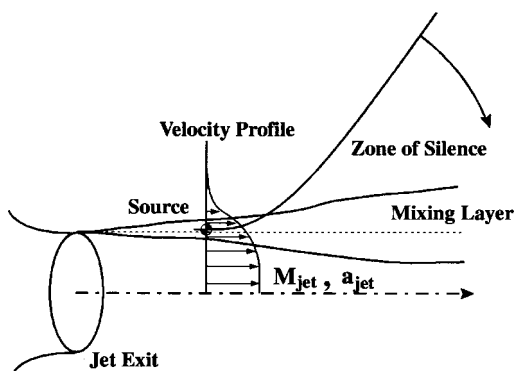

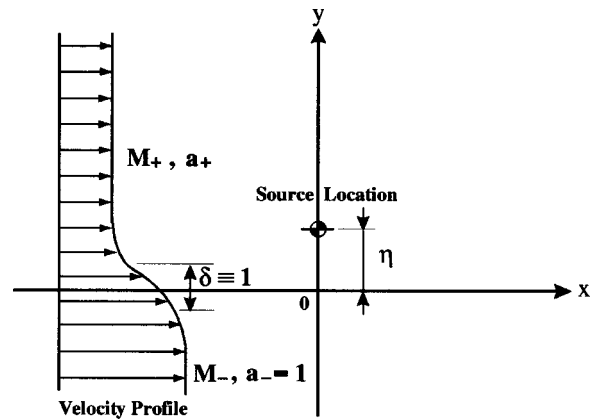FIG. 2. Schematic of the noise from a jet.

end of Sec. IV). Set a monopole (single-frequency) source at $(x,y)=(0,\eta)$ without loss of generality. To solve acoustic fields in transversely sheared flows of this type, the third-order convective wave equation, called Lilley's equation,[10] is adequate. The homogeneous equation can be expressed as follows:

$$\frac{D}{Dt}\left[\frac{D^2\Pi}{Dt^2}-\frac{\partial}{\partial x_j}\left(a^2\frac{\partial\Pi}{\partial x_j}\right)\right]+2\frac{\partial u_k}{\partial x_j}\frac{\partial}{\partial x_k}\left(a^2\frac{\partial\Pi}{\partial x_j}\right)=0, \quad (1)$$

where $D/Dt=(\partial/\partial t)+u_1(\partial/\partial x_1)$ and $\Pi=\gamma^{-1}\log(p/p_\infty)$, p_∞ being the constant mean pressure, and γ the specific heat ratio. Furthermore, assume that (1) is nondimensionalized by taking the vorticity thickness δ to the length scale and the speed of sound at $y=-\infty$, a_-, to be the velocity scale; therefore, u_i denotes the local Mach number times the local speed of sound, and a^2 denotes the local temperature. Based on (1), the amplitude of diffracted waves in the zone of silence, referred to as "refracted arrival waves," is analytically formulated in both low- and high-frequency limits in this section.

A. High-frequency limit (finite thickness model)

When the acoustic wavelength is much shorter than the characteristic length scale of the medium, in the present case the vorticity thickness, one can assume the high-frequency limit and apply geometrical acoustics.[4,7] Assume the acoustic pressure fluctuation to be the following form:

$$\Pi(t,\mathbf{x})=e^{-i\omega t}P(\mathbf{x})\exp[i\omega\phi(\mathbf{x})]. \quad (2)$$

Substitute (2) into (1), and asymptotically expand it with respect to ω. By taking the leading terms of ω, one can obtain the eikonal equation

$$(1-u_j\phi_j)^2-a^2\phi_j^2=0, \quad (3)$$

where $\phi_i\equiv\partial\phi/\partial x_i$, which corresponds to the local wave-number vector. By using the method of characteristics,[4] one can reduce (3) to the following O.D.E. system:

$$\frac{dx_i}{dt}=\frac{a^2}{1-u_k\phi_k}\phi_i+u_i, \quad (4)$$

$$\frac{d\phi_i}{dt} = -\frac{\partial u_k}{\partial x_i}\phi_k - \frac{1 - u_k\phi_k}{2a^2}\frac{\partial a^2}{\partial x_i}, \tag{5}$$

$$\frac{d\phi}{dt} = 1. \tag{6}$$

Notice that the phase ϕ has the same units (actually same scale) as time. Likewise, by taking the second-highest terms of ω, one can derive the first-order transport equation

$$2u_jP_j(1 - u_k\phi_k) + 2a^2P_j\phi_j + \frac{2a^2P\phi_j\phi_k}{1 - u_l\phi_l}\frac{\partial u_k}{\partial x_j}$$

$$-P\left[3\left(u_ju_k\phi_{jk} + \phi_ju_k\frac{\partial u_j}{\partial x_k}\right) - a^2\phi_{jj}\right]$$

$$+P\left[\phi_j\frac{\partial a^2}{\partial x_j} - \frac{\phi_j^2u_k}{1 - u_l\phi_l}\frac{\partial a^2}{\partial x_k} - \frac{2a^2\phi_ju_k\phi_{jk}}{1 - u_l\phi_l}\right] = 0. \tag{7}$$

Here, again $P_i \equiv \partial P/\partial x_i$. To simplify (7), use the following relation obtained by differentiating (3) by D/Dt:

$$2\left(u_ju_k\phi_{jk} + \phi_ju_k\frac{\partial u_j}{\partial x_k}\right) - \frac{2a^2\phi_j\phi_k}{1 - u_l\phi_l}\frac{\partial u_k}{\partial x_j}$$

$$-\left[\phi_j\frac{\partial a^2}{\partial x_j} - \frac{\phi_j^2u_k}{1 - u_l\phi_l}\frac{\partial a^2}{\partial x_k} + \frac{2a^4\phi_j\phi_k\phi_{jk}}{(1 - u_k\phi_k)^2}\right] = 0. \tag{8}$$

Substituting (8) into (7), using (4), and assuming the mean pressure is constant everywhere (hence, $(1/\rho)(D\rho/Dt) + (1/a^2)(Da^2/Dt) = 0$), (7) can be simplified as follows:

$$\frac{\partial}{\partial x_j}\left[\frac{P^2}{1 - u_k\phi_k}\frac{dx_j}{dt}\right] = 0. \tag{9}$$

Hence, the quantity called the "Blokhintzev invariant"[7] is conserved along ray tubes

$$\frac{P^2S}{1 - u_k\phi_k}\left|\frac{d\mathbf{x}}{dt}\right| = \text{Const.}, \tag{10}$$

where S denotes the cross section of the ray tube normal to the ray direction. In the denominator, the mean pressure, which is assumed to be constant, disappears compared with the general expression of the Blokhintzev invariant. This expression will be used later to calculate the amplitude of refracted arrival waves.

Now, when the mean velocity and temperature profiles are purely transversely sheared, the O.D.E. system (4)–(6) can be simplified: $d\phi_x/dt = 0$ in (5). In other words, ϕ_x is constant along the ray. Accordingly, they can be rewritten as follows:

$$\frac{dx}{dt} = \frac{a^2(y)}{1 - M(y)\phi_x}\phi_x + M(y), \tag{11}$$

$$\frac{dy}{dt} = \frac{a^2(y)}{1 - M(y)\phi_x}\phi_y, \tag{12}$$
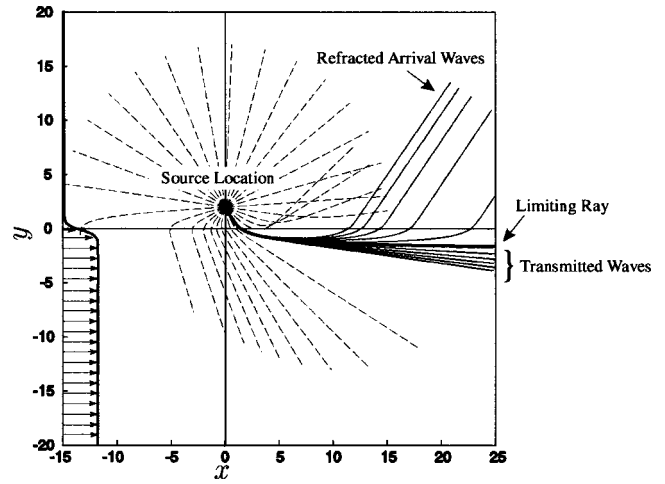
$$\frac{d\phi_x}{dt} = 0, \tag{13}$$

FIG. 4. Ray trajectories from a point source above a mixing layer. The source is located at $(x,y) = (0,2)$, the temperature is constant everywhere, and the velocity profile is given by $M(y) = 0.8[1 - \tanh(2y)]/2$ shown on the left-hand side. The dashed lines are drawn every 3° in all directions, and the solid lines are drawn by the interval of 0.3° near the limiting ray.

$$\frac{d\phi_y}{dt} = -\frac{dM}{dy}\phi_x - \frac{1 - M(y)\phi_x}{2a^2(y)}\frac{da^2}{dy}, \tag{14}$$

$$\frac{d\phi}{dt} = 1. \tag{15}$$

Again, $M(y)$ denotes the velocity profile (not the Mach number) whose reference speed is $a_- = a(-\infty)$.

For convenience, consider the case in which $\phi_x > 0$, and $d\phi_y/dt \geq 0$ along the ray in (14), such as rays propagating downstream above a hot jet. Among these rays, if the initial grazing angle θ is lower than a certain threshold value ($\theta < \theta^\star$, where $\theta^\star$ will be defined later), this ray propagates into the lower side and never appears on the upper side, called a "transmitted wave" in this paper (see Fig. 4). In contrast, if $\theta > \theta^\star$, this ray propagates on the upper side. In particular, when the rays whose grazing angles are only slightly higher than this threshold, they appear as refracted arrival waves departing from the mixing layer to the upper side at nearly the same angles. The ray whose initial grazing angle is exactly $\theta = \theta^\star$ is called a "limiting ray." As Fig. 4 shows, the turning points of the refracted arrival rays, at which the rays become parallel to the mixing layer, are fairly close to the lower free-stream region when the rays are propagating far downstream. Accordingly, these rays propagate horizontally just beneath the mixing layer for long distances. To solve these ray trajectories, assume that the velocity and temperature profiles approach the lower free-stream conditions exponentially. In other words, the velocity and the temperature profiles near the turning points can be approximated by

$$M(y) = M_- - \Delta Me^{\alpha_1 y}, \tag{16}$$

$$a^2(y) = 1 - \Delta a^2e^{\alpha_2 y}, \tag{17}$$

as $y \to -\infty$, where $\alpha_1, \alpha_2 > 0$, and ΔM and Δa^2 are some constants determined from the flow field. In many real physical flows, α_1 and α_2 can be common near the free-stream

region (e.g., the Crocco–Busemann relation: $T \approx -u_1^2/C_p + C_1 u_1 + C_2$, where C_1 and C_2 are constants). Hence, set $\alpha_1 = \alpha_2 = \alpha$. If $\alpha_1 \neq \alpha_2$, just retain the term whose α is smaller. This model should cover realistic flows; however, if the profiles do not follow the formulas (16) and (17), extension of the present method is required, such as curve fitting. Nonetheless, the proportionality of the frequency and the distance from the source should show similar features as discussed at the end of this section. Substitute (16) and (17) into the O.D.E. system (11)–(15), and take the leading-order terms assuming $\Delta M e^{\alpha y}$ and $\Delta a^2 e^{\alpha y}$ to be small. Consequently, one can simplify them as follows:

$$\frac{dx}{dt} \approx \frac{1}{1 - M_- \phi_x} \phi_x + M_-, \tag{18}$$

$$\frac{dy}{dt} \approx \frac{1}{1 - M_- \phi_x} \phi_y, \tag{19}$$

$$\frac{d\phi_x}{dt} = 0, \tag{20}$$

$$\frac{d\phi_y}{dt} \approx \left[\phi_x \Delta M + \frac{(1 - M_- \phi_x)\Delta a^2}{2} \right] \alpha e^{\alpha y}, \tag{21}$$

$$\frac{d\phi}{dt} = 1. \tag{22}$$

Notice that at the leading order, dx/dt becomes constant from (18). Differentiating (19) with respect to t, and substituting (21) into it, yields

$$\frac{d^2 y}{dt^2} \approx \frac{1}{1 - M_- \phi_x} \frac{d\phi_y}{dt} \approx \left[\frac{\phi_x \Delta M}{1 - M_- \phi_x} + \frac{\Delta a^2}{2} \right] \alpha e^{\alpha y}$$

$$\equiv \alpha A e^{\alpha y}, \tag{23}$$

where $A \equiv \phi_x \Delta M/(1 - M_- \phi_x) + (\Delta a^2/2)$, which is constant and assumed to be non-negative along the ray. Redefining $z \equiv e^{\alpha y}$ and substituting it into (23), one can obtain the following O.D.E.:

$$z \frac{d^2 z}{dt^2} - \left(\frac{dz}{dt} \right)^2 - \alpha^2 A z^3 = 0. \tag{24}$$

To reduce (24) to an integrable form, convert the variables by setting $\psi_0 \equiv z$ and $\psi_1 \equiv \dot{z}$. After calculating $d\psi_1/d\psi_0$, (24) yields

$$\frac{d\dot{z}^2}{dz} = \frac{2\dot{z}^2}{z} + 2\alpha^2 A z^2. \tag{25}$$

From (25), the general solution can be obtained as

$$\dot{z}^2 = 2\alpha^2 A z^2 (z \pm \beta^2). \tag{26}$$

Here, β is an arbitrary constant (defined to be $\beta \in [0,\infty)$ here for convenience) always satisfying $z \pm \beta^2 \geq 0$. When one takes the plus sign in (26), it corresponds to a ray of a transmitted wave. In contrast, with the minus sign, $z = \beta^2$ at a certain point, corresponding to a ray of a refracted arrival wave. This point is actually the turning point, which can be expressed as

$$y^* = \frac{2}{\alpha} \log \beta. \tag{27}$$

In this paper, the superscript * denotes the quantity at the turning point. Note that if $\beta = 0$ in (26), it corresponds to the limiting ray.

First, to solve the ray trajectories of refracted arrival waves, take the minus sign in (26), convert the variable by setting $\sqrt{(z - \beta^2)} \equiv \beta \tan \vartheta$ $(0 \leq \vartheta < \pi/2)$, and integrate it. After some calculation, it yields

$$\vartheta = \pm \sqrt{\frac{\alpha^2 \beta^2 A}{2}}(t - t^*). \tag{28}$$

Here, t^* denotes the time when the ray passes through the turning point. Equation (28) indicates that the trajectory is symmetric about the turning point. Rewriting (18) and (28) in the physical domain, one can obtain the ray trajectory near the turning point as follows:

$$x - x^* \approx B(t - t^*), \tag{29}$$

$$y \approx \frac{2}{\alpha} \log \frac{\beta}{\cos[\sqrt{\alpha^2 \beta^2 A/2}(t - t^*)]}. \tag{30}$$

where $B = [M_- + (1 - M_-^2)\phi_x]/(1 - M_- \phi_x)$. Combining (29) and (30), it can be rewritten by

$$y \approx \frac{2}{\alpha} \log \frac{\beta}{\cos[\beta C(x - x^*)]}, \tag{31}$$

where $C = \sqrt{\alpha^2 A/2B^2}$. This equation will be used later to derive the amplitude of refracted arrival waves.

Second, a special solution, the limiting ray, can be obtained by setting $\beta = 0$ in (26). By directly integrating (26), one can obtain

$$y \approx \frac{2}{\alpha} \log \frac{1}{\sqrt{\alpha^2 A/2}(t - t_0)} \approx \frac{2}{\alpha} \log \frac{1}{C(x - x_0)}. \tag{32}$$

Here, x_0 denotes a certain reference point.

Finally, to solve the rays of transmitted waves, take the plus sign in (26), and set $z = \beta^2 \tan^2 \vartheta$ $(0 \leq \vartheta < \pi/2)$. After integrating the equation, one can obtain

$$y \approx \frac{1}{\alpha} \log \frac{\beta^2 (1 - \cos^2 \vartheta)}{\cos^2 \vartheta} \approx \frac{2}{\alpha} \log \frac{\beta}{\sinh[\beta C(x - x_0)]}. \tag{33}$$

Next, consider the trajectory of the turning points for refracted arrival waves propagating far downstream (see Fig. 5). The initial grazing angles of these rays are slightly higher than the angle of the limiting ray; hence, the locations where these rays enter the mixing layer are approximately the same. Here, these locations are called the "incident points," denoted by x_{in} in this paper. On the other hand, due to the slight difference of the initial angles, the distances from the incident points to the turning points are quite different; accordingly, the locations at which the rays depart from the mixing layer are also different. These locations are called the "departing points," denoted by x_{out}. Recalling the ray trajectories are symmetric about the turning points from (28), the

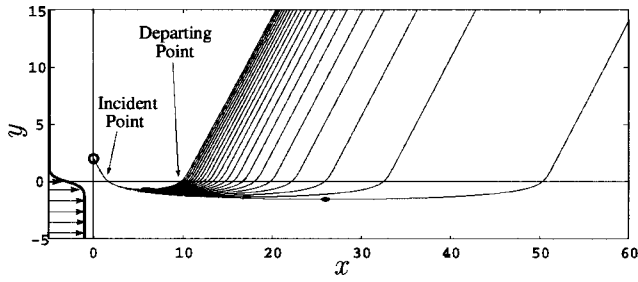Takao Suzuki and Sanjiva Lele: Refracted arrival waves 719

FIG. 5. Example of ray trajectories of refracted arrival waves. The velocity profile is depicted on the left-hand side ($M(y)=0.8[1-\tanh(2y)]/2$), and the temperature is constant everywhere. The source is located at $(x,y)=(0,2)$ (same as Fig. 4). The initial angles of the rays are $-56.25-$ $-55.25°$ with the interval of $0.05°$. Solid dots denote the turning points.

distance from the incident point to the departing point is twice that to the turning point. Now, for the rays propagating far downstream, typically $|\alpha y^*|$ becomes a relatively large value; hence, $\beta = e^{\alpha y^*/2}$ tends to be a fairly small value. For example, when $\alpha y^* = -5$, $\beta = 0.0821$. On the other hand, near the incident point, $y_{in} \approx 0$; accordingly, $\beta/\cos[\beta C(x^*-x_{in})] \approx 1$ from (31). Therefore, since $|\beta| \ll 1$, $|\cos[\beta C(x^*-x_{in})]| \ll 1$ must be satisfied; namely

$$\beta C |x^*-x_{in}| \approx \frac{\pi}{2}. \tag{34}$$

Hence, using (27) the trajectory of the turning point can be approximated by

$$y^* \approx \frac{2}{\alpha} \log \frac{\pi}{2C(x^*-x_{in})}. \tag{35}$$

Now, the pressure amplitude of refracted arrival waves is derived using the Blokhintzev invariant (10). By calculating the departing points of adjacent rays, the amplitude can be approximately solved. First, using (35), calculate the turning points of adjacent rays. Knowing that C is a function of ϕ_x, differentiate (35) as follows:

$$\left[\frac{\alpha(x^*-x_{in})}{2} dy^* + dx^*\right] e^{\alpha y^*/2} \approx -\frac{\pi}{2C^2} \frac{dC}{d\phi_x} d\phi_x. \tag{36}$$

On the other hand, the relation between y^* and ϕ_x can be obtained from the eikonal equation (3). Knowing that $\phi_y = 0$ gives the turning point, differentiate (3) and simplify it as follows:

$$(1-M_-\phi_x)\alpha A e^{\alpha y^*} dy^* - B d\phi_x = 0. \tag{37}$$

Furthermore, from (3), ϕ_x for the limiting ray is given by

$$\phi_x^\star = \frac{1}{1+M_-}. \tag{38}$$

Here, the superscript $\star$ denotes the quantity of the limiting ray. Substituting (35) and (37) into (36) yields

$$\left[\frac{B}{2(1-M_-\phi_x^\star)A} + \frac{\pi^2}{4C^3} \frac{dC}{d\phi_x} (x^*-x_{in})^{-2}\right] d\phi_x$$

$$+ \frac{\pi^2}{4C^2} (x^*-x_{in})^{-3} dx^* \approx 0. \tag{39}$$

Here, the second term in [ ] becomes negligible far downstream (as $|x^*-x_{in}| \to \infty$). Thus, the intensity is proportional to

$$I \sim \frac{d\phi_x}{dx^*} \approx -\frac{\pi^2(1-M_-\phi_x^\star)A}{2BC^2(x^*-x_{in})^3} = -\frac{\pi^2}{\alpha^2}(x^*-x_{in})^{-3}. \tag{40}$$

On the other hand, near the source the cross-section area can be calculated from the difference of the initial grazing angles. From (11) and (12), calculate the change of the ray path with respect to ϕ_x near the source

$$\frac{\partial}{\partial \phi_x}\left(\frac{dx}{dt}\right)_s = \frac{1}{n_s^2}, \tag{41}$$

$$\frac{\partial}{\partial \phi_x}\left(\frac{dy}{dt}\right)_s = \frac{\phi_x}{n_s^2 \sqrt{\bar{n}_s^2-\phi_x^2}}, \tag{42}$$

where the quantities with the subscript s are evaluated at the source point, and $\bar{n} \equiv (1-M\phi_x)/a$. As seen later, $\bar{n}$ behaves as a refraction index. Now, to apply the ray tube theory using (10), it is convenient to calculate the following quantity:

$$\left|\frac{d\mathbf{x}/dt}{1-M(y)\phi_x} \frac{dS}{d\phi_x}\right|_s$$

$$= \frac{\left|\left(\frac{dx}{dt}, \frac{dy}{dt}\right) \times \left(\frac{\partial}{\partial \phi_x}\left(\frac{dx}{dt}\right), \frac{\partial}{\partial \phi_x}\left(\frac{dy}{dt}\right)\right) dt\right|_s}{1-M_s\phi_x}$$

$$= \frac{dt}{a_s \bar{n}_s^3 \sqrt{\bar{n}_s^2-\phi_x^2}}. \tag{43}$$

The distance from the source dr and the time dt is related as

$$\left(\frac{dr}{dt}\right)_s = \sqrt{\left(\frac{dx}{dt}\right)_s^2 + \left(\frac{dy}{dt}\right)_s^2} = a_s\left[\left(1 + \frac{M_s^2}{a_s^2}\right) + 2\frac{M_s\phi_x}{a_s\bar{n}_s}\right]^{1/2}. \tag{44}$$

Likewise, calculate the same quantity at the departing point

$$\left|\frac{d\mathbf{x}/dt}{1-M(y)\phi_x} \frac{dS}{d\phi_x}\right|_{out} = \frac{\left|\left(\frac{dx}{dt}, \frac{dy}{dt}\right)_+ \times \left(\frac{dx_{out}}{d\phi_x}, 0\right)\right|}{1-M_+\phi_x}$$

$$= \frac{\sqrt{\bar{n}_+^{\star 2}-\phi_x^{\star 2}}}{\bar{n}_+^{\star 2}} \frac{dx_{out}}{d\phi_x}. \tag{45}$$

Here, (45) is evaluated in the uniform region right above the mixing layer. Remember that in the upper free-stream region, the rays are almost parallel, and refracted arrival waves propagate in the form of general plane waves.

Now, the solution close to a monopole source can be written as

$$\Pi_s(r) = \frac{1}{2\sqrt{2\pi}} \frac{\exp\left[i\left(\dfrac{-\dfrac{M_s}{a_s}\cos\theta + \sqrt{1 - \dfrac{M_s^2}{a_s^2}\sin^2\theta}}{1 - (M_s^2/a_s^2)} \dfrac{\omega r}{a_s} - \dfrac{3}{4}\pi \right) \right]}{\omega^{1/2} r^{1/2} a_s^{3/2}\left(1 - \dfrac{M_s^2}{a_s^2}\sin^2\theta_s\right)^{1/4}},\tag{46}$$

where $x = r\cos\theta$ and $y = r\sin\theta$. In particular, the initial grazing angle for refracted arrival waves $\theta_s^\star$ is given by

$$\tan\theta_s^\star \equiv \frac{\left(\dfrac{dy}{dt}\right)_s}{\left(\dfrac{dx}{dt}\right)_s} = -\frac{\sqrt{\bar{n}_s^{\star2} - \phi_x^{\star2}}}{\left(1 - \dfrac{M_s^2}{a_s^2}\right)\phi_x^\star + \dfrac{M_s}{a_s^2}},\tag{47}$$

where $\phi_x^\star$ is approximated by (38). The expression (46) can be obtained from (A11) (shown later) by assuming that the flow field near the source is uniform, and taking the limit of a far-field asymptote, $\omega r \to \infty$. Combining (40) and (43)–(46), the amplitude of refracted arrival waves from a finite thickness mixing layer is approximated by

$$
\begin{aligned}
|\Pi_+(\omega, x, y)| &\approx |\Pi_s(dr)| \frac{\sqrt{\left|\dfrac{d\mathbf{x}/dt}{1 - M\phi_x^\star}\dfrac{dS}{d\phi_x}\right|_s}}{\sqrt{\left|\dfrac{d\mathbf{x}/dt}{1 - M\phi_x^\star}\dfrac{dS}{d\phi_x}\right|_{\text{out}}}} \\[2mm]
&= \frac{\left|\dfrac{1}{2}\dfrac{d\phi_x}{dx*}\right|^{1/2}\left(\dfrac{dt}{dr}\right)_s^{1/2}}{2\sqrt{2\pi}\omega^{1/2}a_s^{3/2}\left(1 - \dfrac{M_s^2}{a_s^2}\sin^2\theta_s^\star\right)^{1/4}} \\[2mm]
&\quad \times \frac{\bar{n}_+}{a_s^{1/2}\bar{n}_s^{\star3/2}\sqrt[4]{\bar{n}_s^{\star2} - \phi_x^{\star2}}\sqrt[4]{\bar{n}_+^{\star2} - \phi_x^{\star2}}} \\[2mm]
&= \frac{\sqrt{2\pi}}{2\omega^{1/2}\alpha} \frac{\bar{n}_+^\star}{a_s^2\bar{n}_s^{\star3/2}\sqrt{|\sin\theta_s^\star|}\sqrt[4]{\bar{n}_+^{\star2} - \phi_x^{\star2}}} \\[2mm]
&\quad \times \frac{1}{\left[\left(1 + \dfrac{M_s^2}{a_s^2}\right) + 2\dfrac{M_s\phi_x^\star}{a_s\bar{n}_s^\star}\right]^{1/4} X^{3/2}},
\end{aligned}\tag{48}
$$

where $X \equiv x - (\sqrt{\bar{n}_s^{\star2} - \phi_x^{\star2}}/\phi_x^\star)y$. Here, since the ray trajectory is symmetric about the turning point, it is assumed that $2|x* - x_{\text{in}}| = |x_{\text{out}} - x_{\text{in}}|$. Note when the source is at a large distance from the mixing layer ($\eta \gtrsim 1$), the correction for the distance from the source to the incident point needs to be included [see Eq. (59) shown later]. On the other hand, when the source approaches the lower free-stream region, e.g.,

$\eta \lesssim -1$, the corresponding incident points are no longer identical for the rays of refracted arrival waves, and the approximation fails. This expression (48) will be compared with the expressions based on a vortex sheet as well as the numerical results.

B. Low-frequency limit (vortex sheet model)

When the acoustic wavelength is much longer than the vorticity thickness, a vortex sheet can be used, which corresponds to the low frequency limit. Refracted arrival waves of this type have been reported in several studies.[1–3] In this section, the resultant formulas of refracted arrival waves in the low-frequency limit are shown in two cases (the source is located above and below the vortex sheet). For their derivation, please refer to the Appendix.

When the source is located above the mixing layer ($\eta > 0$), the absolute value of pressure amplitude yields

$$|\Pi_+(\omega, x, y)| \approx \frac{1}{\sqrt{2\pi}\omega^{3/2}} \frac{\bar{n}_+^{\star2}}{a_+^2\bar{n}_-^{\star2}(\bar{n}_+^{\star2} - \phi_x^{\star2})X^{3/2}}.\tag{49}$$

Here the notation is the same as (48), and this expression is valid only in the zone of silence on the upper side. Likewise, when the source is located below the mixing layer ($\eta < 0$)

$$|\Pi_+(\omega, x, y)| \approx \frac{1}{\sqrt{2\pi}\omega^{3/2}} \frac{\bar{n}_+^{\star4}}{\bar{n}_-^{\star4}(\bar{n}_+^{\star2} - \phi_x^{\star2})X^{3/2}}.\tag{50}$$

Note that the expression (50) gives larger amplitude than the expression (49), as shown later. Here, one can see that the decay rate of (49) or (50) for a vortex sheet and that of (48) for a finite thickness mixing layer are common ($X^{-3/2} = [x - \sqrt{(\bar{n}_+^{\star2} - \phi_x^{\star2})}y/\phi_x^\star]^{-3/2}$). However, their coefficients are different. It is important to notice that as the frequency varies, (49) and (50) are proportional to $\sim \omega^{-3/2}$, while (48) is proportional to $\sim \omega^{-1/2}$ with a fixed α. In other words, as the frequency increases with the flow geometry fixed, the amplitude is guaranteed to exceed the prediction based on the vortex sheet model. This proportionality is still valid for the finite thickness mixing layer with the velocity and temperature profiles other than $\sim e^{\alpha y}$. Remember that the ray trajectories are independent of the source frequency so long as the frequency is considered high enough; hence, the only part in which the frequency dependence appears is the amplitude expression near the source (46). These theoretical expressions (48), (49), and (50), are compared with the numerical results in Sec. IV later.

Takao Suzuki and Sanjiva Lele: Refracted arrival waves

III. NUMERICAL SIMULATION

To compare the analytical formulas with more accurate solutions, pressure amplitude of refracted arrival waves is numerically solved based on geometrical acoustics. The procedures are to simply integrate the eikonal equation and to apply the ray-tube theory, which are described in this section.

To solve ray trajectories, the O.D.E. system of the eikonal equation, (11)–(15), was numerically integrated using the standard fourth-order Runge–Kutta scheme. The initial conditions are as follows:

$$x(0) = 0, \tag{51}$$

$$y(0) = \eta, \tag{52}$$

$$\phi_x(0) = \frac{\cos \theta_i}{a_s + M_s \cos \theta_i}, \tag{53}$$

$$\phi_y(0) = \frac{\sin \theta_i}{a_s + M_s \cos \theta_i}, \tag{54}$$

$$\phi(0) = 0, \tag{55}$$

where the initial grazing angle θ_s is given by $\tan \theta_s \equiv a_s \sin \theta_i / (M_s + a_s \cos \theta_i)$. For simplicity, the velocity profile was set to be

$$M(y) = \frac{M_-}{2} [1 - \tanh(2y)] \qquad (M_- > 0). \tag{56}$$

This formula provides $M(y) \to M_- - M_- e^{4y}$ as $y \to -\infty$, which is consistent with (16) ($M_+ = 0.$, $\Delta M = M_-$, and $\alpha = 4.$). In addition, this velocity profile yields the vorticity thickness of $\delta \equiv \Delta M / (dM/dy)_{max} = 1$. Similarly, the temperature profile was set to be

$$a^2(y) = \frac{1 - a_+^2}{2} [1 - \tanh(2y)] + a_+^2. \tag{57}$$

It also yields $a^2(y) \to 1 - (1 - a_+^2) e^{4y}$ as $y \to -\infty$. If $a_+^2 < 1$, the flow corresponds to a hot jet, while if $a_+^2 > 1$, it corresponds to a cold jet. [In this case, M_- must be reasonably large so that A is always non-negative. See Eq. (23).]

Once the ray trajectories were computed, the Blokhintzev invariant (10) was used to obtain pressure amplitude by calculating cross sections between adjacent rays. Defining (x_n, y_n) to be a certain grid point of the nth ray, the infinitesimal cross section of the nth ray was computed by the following midpoint rule:

$$dS_n \approx \frac{\left| (x_{n+1} - x_{n-1}, y_{n+1} - y_{n-1}) \times \left(\frac{dx}{dt}, \frac{dy}{dt} \right)_n \right|}{2 \sqrt{\left(\frac{dx}{dt} \right)_n^2 + \left(\frac{dy}{dt} \right)_n^2}}, \tag{58}$$

where dx/dt and dy/dt were given by (11) and (12), respectively. A total of 100 rays was issued with the interval of $\Delta \theta_i = 0.005°$ from the angle of the limiting ray. The time step was taken to be $dt = 0.025 (\times \delta/a_-)$. The ratio of the infinitesimal cross section at the grid closest from the source to that at the grid right above $y = 2$ (almost uniform flow) was used to calculate amplitude. In addition, the amplitude near the source point was calculated using (46), which is
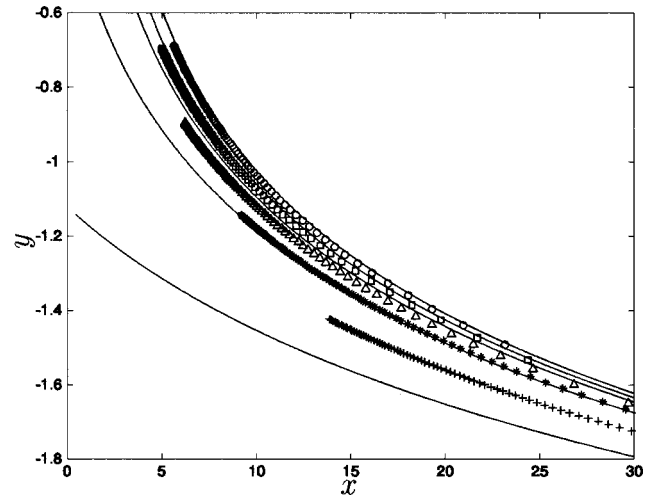

FIG. 6. Turning-point trajectories for different source locations. The lower free-stream velocity is $M_- = 0.8$, and the temperature is constant everywhere. Symbols were computed by numerical integration: $\bigcirc$, $\eta = 2$; $\square$, $\eta = 1$; $\triangle$, $\eta = 0$; $*$, $\eta = -0.5$; and $+$, $\eta = -1$. Lines were calculated using (35) corresponding to $\eta = 2, 1, 0, -0.5$, and -1 from the top.

consistent with the analytic expression. Thus, pressure amplitude of refracted arrival waves was numerically calculated based on the ray-tube theory.

IV. RESULTS AND DISCUSSION

A. Turning point trajectory

First, to observe the accuracy of the analytical expression, turning-point trajectories were calculated using both analytical expression (35) and numerical integration (11)–(15), and the results are compared. Here, the incident locations in (35) were approximated by the following form:

$$x_{in} = -\frac{\eta}{\tan \theta_s^\star}, \tag{59}$$

where $\theta_s^\star \in [-\pi/2, 0)$ is defined by (47).

Figure 6 represents the dependence of the turning-point trajectories on the source location. It shows that as the source location becomes lower (closer to the higher velocity side), the trajectories shift downward. When $\eta \geq -0.5$, the theoretical predictions agree with the numerical solutions fairly well. But, when the source location approaches the lower free-stream ($\eta = -1.$ case), the theoretical prediction deviates far lower than the numerical solution. Remember that the formula (35) assumes the incident points of the rays to be identical; hence, when the source approaches the lower free-stream region, this expression tends to fail. Nonetheless, the analytical expression approximates the ray trajectories fairly well when the source is above or close to the center line of the mixing layer.

Figure 7 represents the dependence of the ray trajectories on the lower free-stream velocity. (Although M_- actually yields the Mach number of the lower free-stream, the term "free-stream velocity" is used instead of "free-stream Mach number" to emphasize that $M(y)$ denotes the velocity normalized by a_- as opposed to the local Mach number.) This figure indicates that the analytical expression covers a

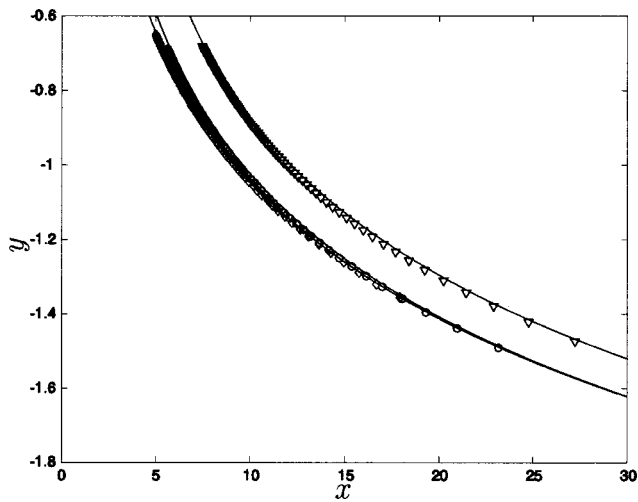Takao Suzuki and Sanjiva Lele: Refracted arrival waves

FIG. 7. Turning-point trajectories for different lower free-stream velocities. The source location is $\eta=2$, and the temperature is constant everywhere. Symbols were computed by numerical integration: $\triangledown$, $M_-=0.3$; $\bigcirc$, $M_- =0.8$; and $\diamondsuit$, $M_-=1.5$. Lines were calculated using (35) corresponding to $M_-=0.3$, 0.8, and 1.5 from the top. Two cases ($M_-=0.8$ and 1.5) almost overlap.

wide velocity range. Thus, one can expect that the analytic expression provides a good approximation to the ray trajectories as long as the source is above or close to the center line of the mixing layer.

B. Pressure amplitude distribution

To validate the analytical expression for various lower free-stream velocities and source locations, pressure amplitude of refracted arrival waves was calculated using (48), and it is compared with the numerical integration using (10) and (11)–(15).

Figures 8(a)–(c) represent the amplitude profiles in the x direction for different lower free-stream velocities and source locations. As seen in Fig. 7, the theoretical predictions and the numerical results agree very well when the source is $\eta \geqslant -0.5$. Hence, one can expect that this expression can be used to estimate the noise generated inside the mixing layer and propagating in the zone of silence. Since the analytical formula (48) assumes a far-field asymptote, the theory and the numerical result agree better as X increases in all cases. Each figure shows that as the source approaches the lower free stream (η decreases), the amplitude increases; in particular, when the source is below $y=0$, the amplitude seems to be fairly sensitive to the source location. This series of figures also indicates that the noise from nearly the lower free stream tends to be strongly amplified as the velocity increases.

C. Comparison between the finite thickness mixing layer model and the vortex sheet model

Next, two analytical models, the finite thickness mixing layer and the vortex sheet models, are compared. Remember that the finite thickness mixing layer model (48) corresponds to the high-frequency limit, while the vortex sheet models (49) and (50), correspond to the low-frequency limit. Figures 9(a)–(c) represent the comparison of these models at differ-
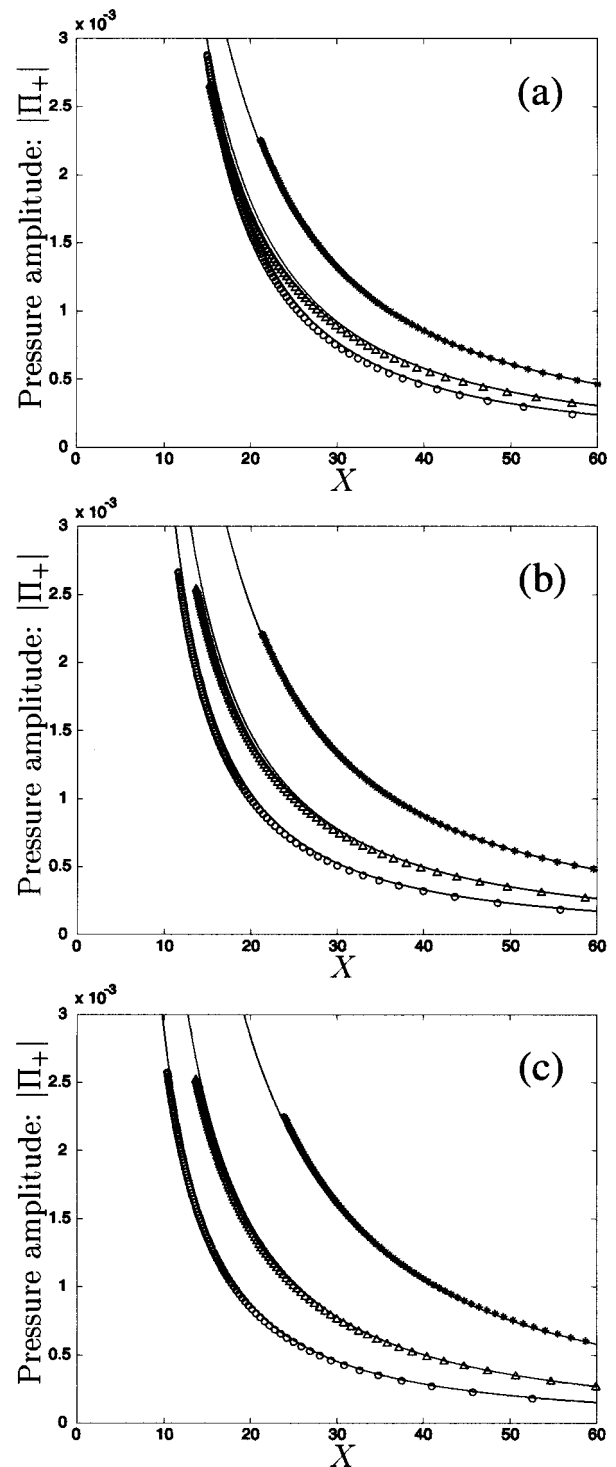

FIG. 8. Comparison of pressure amplitude between the finite thickness mixing layer model and the numerical integration. The amplitudes at $y=2$ are plotted. The lower free-stream velocity is (a) $M_-=0.3$; (b) $M_-=0.8$; and (c) $M_-=1.5$. The temperature is constant everywhere. Symbols were computed by numerical integration: $\bigcirc$, $\eta=2$; $\triangle$, $\eta=0$; and *, $\eta=-0.5$. Lines were calculated using (48) corresponding to $\eta=2, 0$, and 0.5 from the bottom.

ent lower free-stream velocities. Both models show that the amplitude increases as the source approaches the lower free stream. Moreover, all these cases show that as the frequency increases, the amplitude of the finite thickness model exceeds that of both vortex sheet models, as mentioned before.
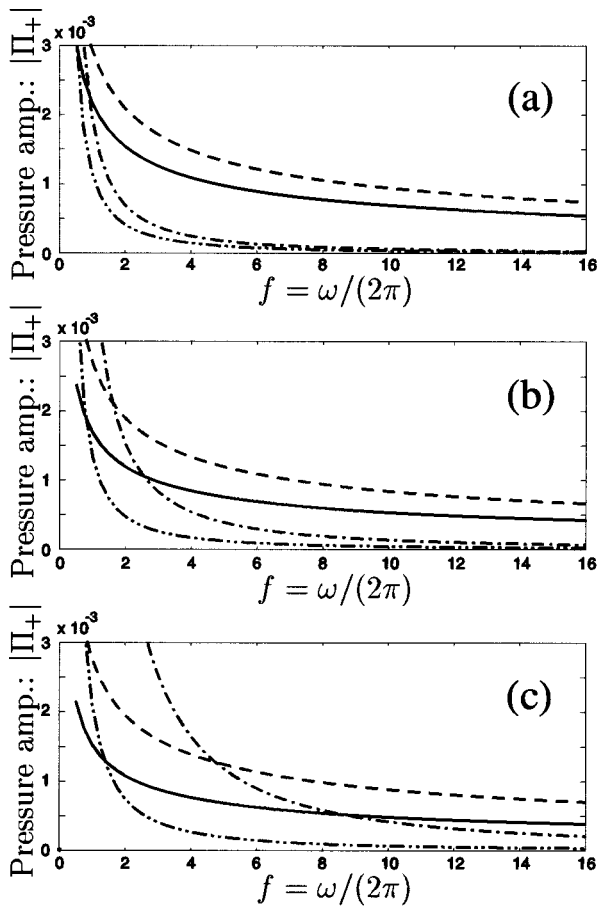
FIG. 9. Comparison between the finite thickness mixing layer model and the vortex sheet models in different lower free-stream velocities. The pressure amplitudes above the mixing layer are plotted. The lower free-stream velocity is (a) $M_- = 0.3$; (b) $M_- = 0.8$, and (c) $M_- = 1.5$. The temperature is constant, and $X = 20$. Lines represent as follows: ——, finite thickness model (48) with $\eta = 2$; - - -, that with $\eta = 0$; $- \cdot \cdot -$, vortex sheet model with the source above the mixing layer (49); and $- \cdot -$, the source below the mixing layer (50).
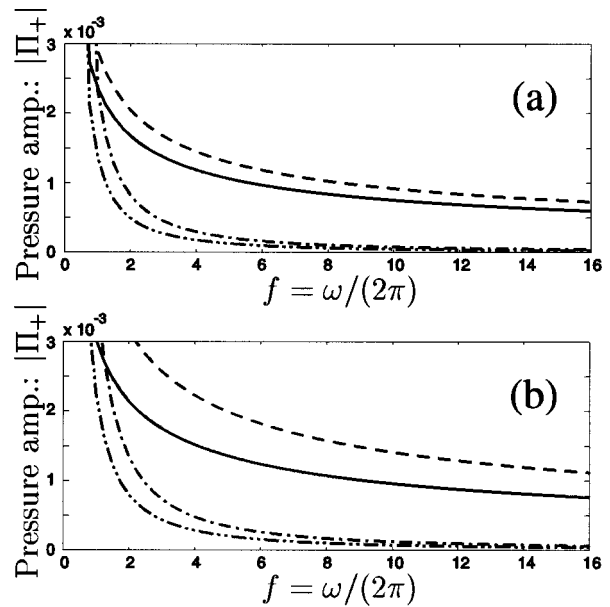

FIG. 10. Comparison between the finite thickness mixing layer model and the vortex sheet models in different speeds of sound. The speed of sound on the upper side is (a) $a_+ = 0.7$ and (b) $a_+ = 1.2$. The lower free-stream velocity is $M_- = 0.3$. The rest of the conditions and notations are the same as Fig. 9.

This tendency is particularly striking in lower subsonic flows. Figure 9(a) clearly demonstrates that the vortex sheet model far underestimates the amplitude of refracted arrival waves in a wide range on the higher-frequency side. Remember that as the frequency increases, the finite thickness model decays as $\sim \omega^{-1/2}$, while the vortex sheet model as $\sim \omega^{-3/2}$.

Figures 10(a) and (b) show the comparison of these models at different speeds of sound. Here, (a) represents a hot jet and (b) a cold jet, and the constant temperature case corresponds to Fig. 9(a). They show that in the vortex sheet model, the temperature variation hardly affects the pressure amplitude. In contrast, in the finite thickness model, the amplitude strongly increases as the source approaches the lower free stream in cold jets; however, it barely changes in hot jets. Notice that due to the definition of the source term $(\hat{\Pi}'' + [n_s^2 - k^2]\hat{\Pi} \sim \delta(y - \eta)/a_s^2$, refers to (A1) shown in the Appendix), the amplitude may even decrease as the source approaches the core of hot jets though the distance between the adjacent rays become narrower. These tendencies will be summarized in the next figures.

Finally, to observe the dependence on the lower free-stream velocity and the speed of sound, the amplitude of

refracted arrival waves was mapped onto the M_- and a_+ plane. Figures 11(a)–(c) represent the pressure amplitude contours calculated by the finite thickness model (48). The regions where contour lines are missing (the left top corner) indicate that refracted arrival waves do not or barely exist under such conditions: $\bar{n}_s^{\star 2} - \phi_x^{\star 2}$ approaches zero in (48). Hence, there are no rays which initially propagate downward and get refracted upward. This series of figures demonstrates the features observed in Figs. 8(a)–(c): As the source approaches the lower free stream, the amplitude tends to increase over the whole range; particularly, this tendency becomes striking when the source is below the center line of the mixing layer ($\eta \lesssim -0.5$). Figure 11 also reveals that the amplitude becomes more sensitive to the lower free-stream velocity as η decreases. They also show that as the jet becomes hotter (a_+ decreases), the amplitude increases in the supersonic range ($M_- \gtrsim 1$) in all cases. On the other hand, in low subsonic flows the amplitude becomes fairly large when the jet becomes colder (a_+ increases). In this region, the critical angle $\theta_s^{\star}$ defined by (47) becomes considerably shallow so that wide angles of the rays are captured within the mixing layer, and the distinction between direct waves and refracted arrival waves becomes ambiguous.

For reference, Fig. 12 represents the amplitude contours calculated using the vortex sheet models for the source (a) above and (b) below the mixing layer, respectively. Note that the direct comparison of the magnitude between Figs. 11 and 12 may not be meaningful, since the amplitude ratio between them depends on the ratio of α/ω. Figures 11(b) and 12(a) as well as Figs. 11(c) and 12(b) show some qualitative similarities. However, when the source is below the mixing layer, the vortex sheet model indicates that the amplitude substantially increases as the velocity increases.

It is important to notice that the solution for refracted

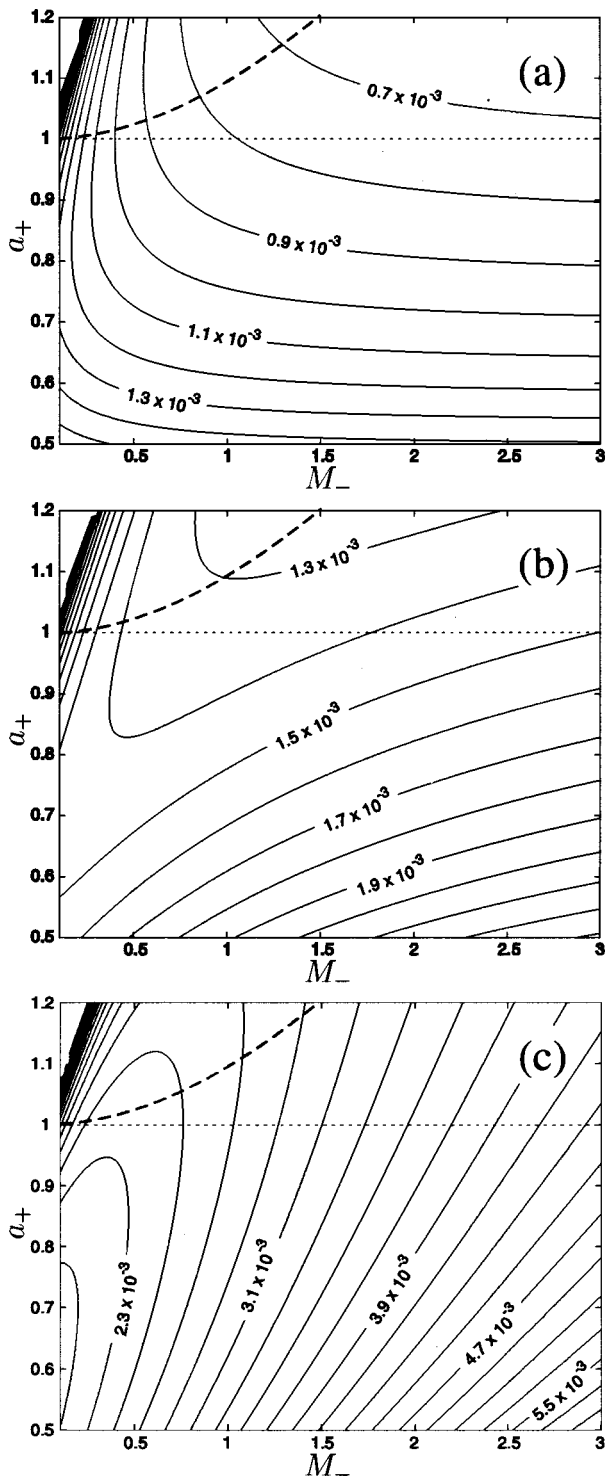Takao Suzuki and Sanjiva Lele: Refracted arrival waves

FIG. 11. Pressure amplitude contours in the plane of the lower free-stream velocity and the speed of sound based on the finite thickness mixing layer model. The pressure amplitudes of the finite thickness model (48) are shown. $\omega/2\pi=4$ and $X=20$. The source is set to be (a) $\eta=2$; (b) $\eta=0$; and (c) $\eta=-0.5$. The thicker dashed line denotes the isoenthalpy line.
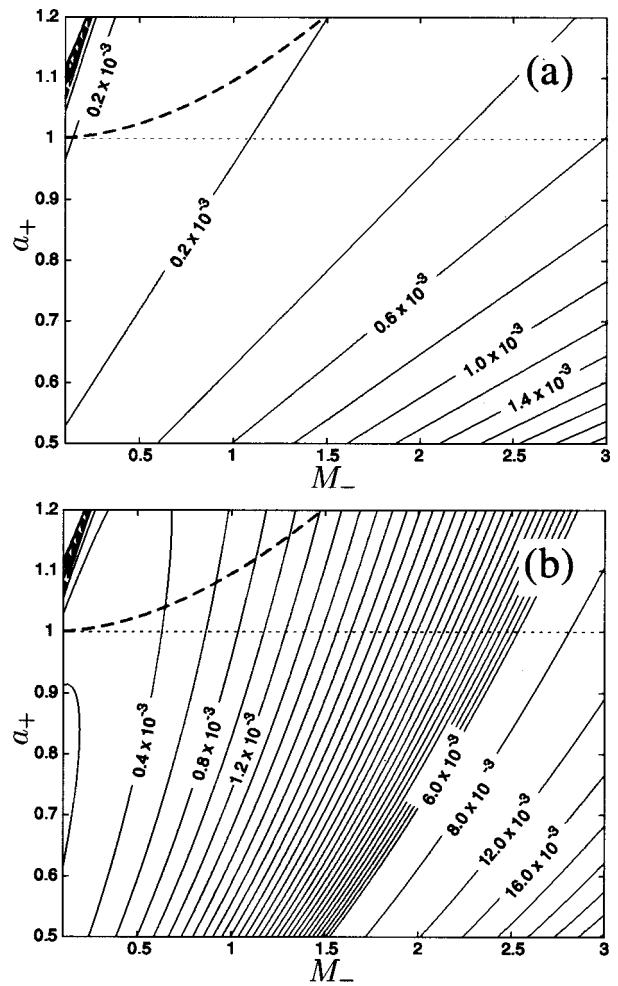

FIG. 12. Pressure amplitude contours in the plane of the lower free-stream velocity and the speed of sound based on the vortex sheet model. The conditions and notations are the same as Fig. 11. The source location is (a) above the mixing layer (49), and (b) below the mixing layer (50).

layer have a similar feature of Mach waves studied in some previous works.[11–13] However, it is worthwhile to observe that supersonic phase velocity can be obtained not only by sources supersonically convected: Waves issued from an upstream source and refracted near the lower free stream have phase velocity of u_-+a_- (where u_- denotes the jet velocity); hence, they can propagate in the zone of silence although the intensity of refracted arrival waves tends to be fairly small, as Figs. 11 and 12 indicate.

It should also be emphasized that the present analysis is based on a parallel mixing layer. Of course, when the jet is spreading,[14] the turning points shift closer to the core; as a result, refracted arrival waves become "more like direct waves" and their amplitude is enhanced (refer to Ref. 15 for calculation in a more realistic flow geometry). Hence, the high-frequency sound in the zone of silence measured in experiments might be caused mainly by direct waves from the end of the potential core.[6] To estimate the mixing layer spreading effect on the sound radiation field, the pressure amplitude was numerically calculated at different spreading rates. The velocity profile was set to be

$$M(x,y)=\frac{M_-}{2}\left[1-\tanh\left(\frac{2y}{1+\delta'x}\right)\right],\qquad(60)$$

arrival waves belongs to the same family as Mach wave-type sound.[11] From a one-dimensional point of view, namely the linear analysis based on (A1), this family satisfies the boundary conditions of exponential decay toward the lower side (high speed) and oscillation toward the upper side (low speed), and changes its nature at the turning point. In this sense, refracted arrival waves from a finite thickness mixing
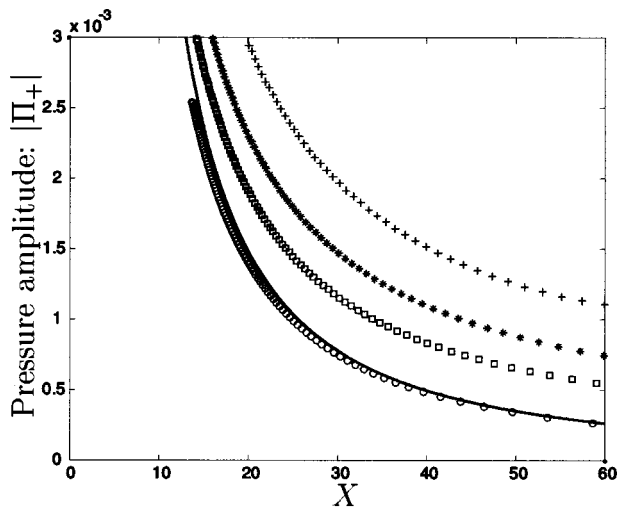
FIG. 13. Comparison of pressure amplitude profile of different spreading rates. The lower free-stream velocity is $M_- = 0.8$, the source location is $\eta = 0$, and the temperature is constant everywhere. Symbols were computed by numerical integration: $\bigcirc$, $\delta' = 0$; $\square$, $\delta' = 0.05$; $*$, $\delta' = 0.10$; and $+$, $\delta' = 0.20$. A solid line was calculated using the finite thickness mixing layer model (48).

where the free-stream velocity was set to be $M_- = 0.8$ and the temperature to be constant everywhere. Here, the source was placed at the origin. The results are plotted in Fig. 13 and compared with the parallel mixing layer model at high frequencies. Figure 13 clearly shows that even $\delta' = 0.1$ of the spreading rate yields several times as large pressure amplitude as that in the parallel mixing layer case. Note that previous experimental and numerical studies (summarized in Ref. 16) have indicated that the spreading rate can be up to $\delta' \sim 0.2$ as the jet Mach number decreases. Therefore, to compare these theoretical expressions with actual experiments, one needs the information about the mean flow as well as rigorous source models and their distribution.

Furthermore, in terms of the frequency range, the most unstable mode of instability waves is likely to be somewhere in between the low- and high-frequency limits. The high-frequency formula derived here focuses on noise due to rather finer scale turbulence. As observed by experiments,[9] the high-frequency component of the jet noise is mainly generated near the nozzle lip, in which large-scale vortical disturbances have not yet significantly grown. In addition, a numerical study by Suzuki[17] shows that this high-frequency formula for refracted arrival waves is applicable when the ratio of the acoustic wavelength to the vorticity thickness becomes unity or less. Therefore, the analysis in this study is expected to be useful for noise generated near the jet exit. However, once instability waves have developed into large-scale vortical structures downstream, such as at the end of the potential core, the current analysis would no longer be valid. Other issues associated with jet noise, such as the multipole and moving sources, are also discussed in Ref. 17.

V. CONCLUSION

Through this study, refracted arrival waves propagating in the zone of silence are formulated in the high-frequency limit and compared with the formula in the low-frequency

limit. These formulas show that the amplitude at high frequencies is proportional to $\omega^{-1/2}$, while that at low frequencies is proportional to $\omega^{-3/2}$, ω being the source angular frequency. This indicates that the existing low-frequency formula,[2,3] namely the vortex sheet model, tends to underestimate the sound-pressure level in the zone of silence as the frequency increases. It also implies that the previous high-frequency theory[8] ignoring refracted arrival waves does not correctly represent the sound radiation pattern in the zone of silence.

This high-frequency formula of refracted arrival waves has significant implications for the application to jet noise. In most previous studies, general plane-wave-type radiation has been considered only for supersonic jet flows (referred to as Mach waves). However, this study indicates that even in subsonic mixing layers, general plane-wave-type sound can theoretically propagate in the zone of silence. In particular, this formula is expected to be applicable to the high-frequency noise mainly generated near the nozzle lip of the jet exit. Therefore, it should be used to estimate the sound-pressure level in the zone of silence at high frequencies. However, at present the existence of such waves in real flows is uncertain, and as noted below, some extensions of the present theory are required for quantitative prediction.

For example, one may need to more rigorously analyze some additional effects of real flows: As the mixing layer spreads, more rays are trapped inside of it and the distinction between refracted arrival waves and direct waves becomes ambiguous. In fact, this study shows that a slight increase in the spreading rate of the mixing layer drastically enhances the amplitude of refracted arrival waves. Other examples which are not studied here are effects of unsteady flow disturbances, source models for turbulent mixing noise, and so on. Nonetheless, it is important to note this study demonstrates that sound radiation pattern in the zone of silence is fundamentally different from the region in which direct waves propagate and the amplitude of refracted arrival waves is different several times over between the low- and high-frequency limits.

ACKNOWLEDGMENTS

APPENDIX: Derivation for the low-frequency limit

To rederive the formulas of refracted arrival waves in the low-frequency limit, derivative matching[4] is used here. First, take a Fourier transform of (1) in time and the flow direction, and set a delta function at $y = \eta$,

$$\frac{\partial}{\partial y}\left(a^2 \frac{\partial \hat{\Pi}}{\partial y}\right) + \frac{2k\frac{\partial M}{\partial y}}{\omega - kM}\left(a^2 \frac{\partial \hat{\Pi}}{\partial y}\right) + [(\omega - kM)^2 - a^2 k^2]\hat{\Pi}$$
$$= \delta(y - \eta), \tag{A1}$$

where

Takao Suzuki and Sanjiva Lele: Refracted arrival waves

$$\hat{\Pi}(\omega,k,y)=\frac{1}{(2\pi)^2}\int_{-\infty}^{\infty}\int_{-\infty}^{\infty}\Pi(t,x,y)e^{i(\omega t-kx)}dt\,dx. \tag{A2}$$

When the wavelength is much longer than the vorticity thickness, the third term of (A1) becomes much smaller than the first two terms. Therefore, in the low-frequency limit (A1) can be approximated by

$$\frac{\partial}{\partial y}\left[\frac{a^2(y)}{(\omega-kM(y))^2}\frac{\partial\hat{\Pi}}{\partial y}\right]\approx\frac{\delta(y-\eta)}{(\omega-kM(y))^2}. \tag{A3}$$

Hence, the quantity $[a^2(y)/(\omega-kM(y))^2]\partial\hat{\Pi}/\partial y$ is constant across the vortex sheet. Subsequently, assuming $|\partial\hat{\Pi}/\partial y|$ is finite, it can be shown that $\hat{\Pi}$ is continuous across the vortex sheet. Although the pressure itself is continuous across the vortex sheet, the first derivative has a discontinuity. Thus, the jump conditions across the vortex sheet become

$$\hat{\Pi}_+(y=0_+)=\hat{\Pi}_-(y=0_-), \tag{A4}$$

$$\frac{1}{n_+^2}\left.\frac{\partial\hat{\Pi}_+}{\partial y}\right|_{y=0_+}=\frac{1}{n_-^2}\left.\frac{\partial\hat{\Pi}_-}{\partial y}\right|_{y=0_-}, \tag{A5}$$

where $n_{\pm}\equiv(\omega-kM_{\pm})/a_{\pm}$, which is equivalent to $\omega\bar{n}_{\pm}$ [$\bar{n}$ is defined after (41) and (42)]. Likewise, k is equal to $\omega\phi_x$ used in the high-frequency limit.

To derive the formulas for refracted arrival waves, first put the source above the vortex sheet ($\eta>0$). In the transverse direction, incident and reflected waves propagate on the upper side, and transmitted waves on the lower side. Knowing that the second term of (A1) vanishes in the uniform flow region, the forms of the solution on the upper and lower sides can be expressed as follows:

$$\hat{\Pi}_+=\frac{e^{-i\sqrt{n_+^2-k^2}(y-\eta)}}{i2a_+^2\sqrt{n_+^2-k^2}}+\mathbf{C}_re^{i\sqrt{n_+^2-k^2}y}, \tag{A6}$$

$$\hat{\Pi}_-=\mathbf{C}_te^{-i\sqrt{n_-^2-k^2}y}. \tag{A7}$$

Here, $\mathbf{C}_r$ and $\mathbf{C}_t$ ($\in\mathbf{C}$) are the reflection and transmission coefficients, respectively. Note that the "resonance mode"[3,18] is not taken into account here for simplicity. Substituting (A6) and (A7) into (A4) and (A5), transmitted waves can be obtained as follows:

$$\hat{\Pi}_-=\frac{e^{i\sqrt{n_+^2-k^2}\eta}e^{-i\sqrt{n_-^2-k^2}y}}{ia_+^2n_+^2\left(\frac{\sqrt{n_+^2-k^2}}{n_+^2}+\frac{\sqrt{n_-^2-k^2}}{n_-^2}\right)}. \tag{A8}$$

By taking an inverse Fourier transform of (A8), the two-dimensional formula can be derived as

$$\Pi_-(\omega,r,\theta)=\frac{1}{2\pi i}\int_{-\infty}^{+\infty}\frac{e^{i\sqrt{n_+^2-k^2}\eta}e^{i(k\cos\theta-\sqrt{n_-^2-k^2}\sin\theta)r}}{a_+^2n_+^2\left(\frac{\sqrt{n_+^2-k^2}}{n_+^2}+\frac{\sqrt{n_-^2-k^2}}{n_-^2}\right)}dk. \tag{A9}$$

To evaluate (A9), assume $\eta\ll r$ and $r\gg1$, and use the stationary phase method. Defining the phase part to be $\varphi(k)\equiv k\cos\theta-\sqrt{(n_-^2-k^2)}\sin\theta$, $\varphi'(k)=0$ gives the stationary point, which becomes

$$k=\frac{\omega}{1-M_-^2}\left(-M_-+\frac{\cos\theta}{\sqrt{1-M_-^2\sin^2\theta}}\right). \tag{A10}$$

As a result, (A9) can be approximated in the far field as follows:

$$\Pi_-(\omega,r,\theta)\approx\frac{\omega^{1/2}}{\sqrt{2\pi}r^{3/2}}\frac{|r\sin\theta|}{(1-M_-^2\sin^2\theta)^{3/4}}\frac{e^{i\sqrt{n_+^2-k^2}\eta}e^{i[-M_-\cos\theta+\sqrt{1-M_-^2\sin^2\theta}/1-M_-^2]\omega r-(3/4)\pi)}}{a_+^2n_+^2\left(\frac{\sqrt{n_+^2-k^2}}{n_+^2}+\frac{\sqrt{n_-^2-k^2}}{n_-^2}\right)}, \tag{A11}$$

where k and $n_{\pm}$ are evaluated at the stationary point (A10). The solution for refracted arrival waves must match with (A11) across the mixing layer. To apply the derivative matching (A5), differentiate (A11) with respect to y and set $y=0$

$$\left.\frac{\partial\Pi_-}{\partial y}\right|_{y=0}\approx\frac{-\omega^{1/2}e^{i\sqrt{n_+^2-k^2}\eta}}{\sqrt{2\pi}x^{3/2}}\frac{e^{i(kx-(3/4)\pi)}}{a_+^2\sqrt{n_+^2-k^2}}. \tag{A12}$$

Here, the stationary point is $k(\theta=0)=\omega/(1+M_-)$.

On the other hand, refracted arrival waves on the upper side should be expressed in the form of general plane waves; hence, they can be written by

$$\Pi_+(\omega,x,y)\approx\mathbf{A}_+\left(x-\frac{\sqrt{n_+^2-k^2}}{k}y\right)e^{i(kx+\sqrt{n_+^2-k^2}y)}. \tag{A13}$$

Similarly, differentiate (A13) with respect to y and evaluate at $y=0$ retaining the lowest order of x (namely, the $\mathbf{A}'_+$ term is eliminated)

$$\left.\frac{\partial\Pi_+}{\partial y}\right|_{y=0}\approx i\sqrt{n_+^2-k^2}\mathbf{A}_+(x)e^{ikx}. \tag{A14}$$

Substituting (A12) and (A14) into (A5), it yields as follows:

$$\Pi_{+}(\omega,x,y) \approx \frac{\omega^{1/2}}{\sqrt{2\pi}} \frac{n_{+}^2}{a_{+}^2 n_{-}^2 (n_{+}^2 - k^2)}$$

$$\times \frac{e^{i\sqrt{n_{+}^2 - k^2}\,\eta} e^{i(kx + \sqrt{n_{+}^2 - k^2}\,y - (\pi/4))}}{\left(x - \frac{\sqrt{n_{+}^2 - k^2}}{k}\,y\right)^{3/2}}.$$

$$(A15)$$

One can obtain the same result by taking a contour integral of (A9). By using the same notation as (48), the absolute value of (A15) becomes (49).

Likewise, put the source below the vortex sheet ($\eta < 0$), and follow the same procedure as described above. It is noticed that there exist incident waves and reflected waves on the lower side, but only the reflected waves contribute the derivative matching. Consequently, the absolute value of pressure amplitude for refracted arrival waves becomes (50) in this case.

[1] P. Gottlieb, "Sound source near a velocity discontinuity," J. Acoust. Soc. Am. **32**, 1117–1123 (1960).

[2] A. B. Friedland and A. D. Pierce, "Reflection of acoustic pulses from stable and instable interfaces between moving fluids," Phys. Fluids **12**(6), 1148–1159 (1969).

[3] M. S. Howe, "Transmission of an acoustic pulse through a plane vortex sheet," J. Fluid Mech. **43**(2), 353–367 (1970).

[4] J. B. Keller and R. M. Lewis, "Asymptotic methods for partial differential equations: The reduced wave equation and Maxwell's equations," in *Surveys in Applied Mathematics*, edited by J. B. Keller, D. W. McLaughlin, and G. C. Papanicolaou (Plenum, New York, 1995), Vol. 1, pp. 1–82.

[5] L. D. Landau and E. M. Lifshitz, *Fluid Mechanics*, Trans., 2nd ed. (Pergamon, New York, 1987), pp. 276–281.

[6] H. K. Tanna, "An experimental study of jet noise. I. Turbulent mixing noise," J. Sound Vib. **50**(3), 405–428 (1977).

[7] D. I. Blokhintzev, "Acoustics of a nonhomogeneous moving medium," Trans., NACA TM 1339 (1946).

[8] M. E. Goldstein, "High frequency sound emission from point multiple sources embedded in arbitrary transversely sheared mean flows," J. Sound Vib. **80**, 499–522 (1982).

[9] B. R. Dougherty, "Phased array beamforming for aeroacoustics," Lecture Notes in an AIAA Professional Development Short Course, 1999.

[10] G. M. Lilley, "On the noise from jets," AGARD, CP-13, 1–12 (1974).

[11] C. K. W. Tam and D. E. Burton, "Sound generated by instability waves of supersonic flows. I. Two-dimensional mixing layer," J. Fluid Mech. **138**, 249–271 (1984).

[12] J. E. Ffowcs Williams, "The noise from turbulence convected at high speed," Philos. Trans. R. Soc. London, Ser. A **255A**, 469–503 (1963).

[13] T. F. Balsa, "The far field of high frequency convected singularities in sheared flows, with an application to jet-noise prediction," J. Fluid Mech. **74**(2), 193–208 (1976).

[14] L. K. Schubert, "Numerical study of sound refraction by a jet flow. I. Ray acoustics," J. Acoust. Soc. Am. **51**, 439–446 (1972).

[15] C. K. W. Tam and L. Auriault, "Mean flow refraction effects on sound radiated from localized sources in a jet," J. Fluid Mech. **370**, 149–174 (1998).

[16] J. B. Freund and S. K. Lele, "Computer simulation and prediction of jet noise," to appear in High Speed Jet Flows, edited by G. Raman, D. K. McLaughlin, and P. J. Morris (Taylor & Francis, London, 2002).

[17] T. Suzuki, "Acoustic wave propagation in transversely sheared flows," Ph.D. dissertation, Stanford University, 2001.

[18] J. W. Miles, "On the reflection of sound at an interface of relative motion," J. Acoust. Soc. Am. **29**(2), 226–228 (1957).